IRANIAN JOURNAL OF CATALYSIS

Investigation on the Photocatalytic and Antibacterial Activities of Green synthesized Cupric Oxide Nanoparticles using *Clitoria ternatea*

S. Prabhu[a,b] *, T. Daniel Thangadurai[c], P. Vijai Bharathy[d], Pon. Kalugasalam[e]

a) Department of Research and Development, Bharathiar University, Coimbatore, Tamil Nadu, India

b) Department of Physics, Hindusthan College of Engineering and Technology, Coimbatore, Tamil Nadu, India

c) Department of Chemistry, KPR Institute of Engineering and Technology, Coimbatore, Tamil Nadu, India

d) Department of Physics, C.B.M College, Coimbatore, Tamil Nadu, India.

e) Department of Physics, Anna University Regional Campus, Coimbatore, Tamil Nadu, India.

ABSTRACT

Green synthesis of cupric oxide nanoparticles (CuO NPs) has been promoted as an environmentally-friendly, cost-effective and high yield method. The CuO NPs have been synthesized by reducing copper sulphate using an aqueous flower extract of *Clitoria ternatea*. The UV-visible peak observed at 251 nm confirmed the formation of CuO NPs. The optical bandgap energy value of CuO NPs was found to be 2.16 eV. The presence of Cu-O band at 490 cm^{-1} in the FTIR spectrum confirms the formation of the CuO NPs. The XRD exhibits monoclinic structure with an average crystallite size of 17.46 nm. The negative zeta potential value (-17.7 mV) demonstrated the stability of CuO NPs. The formation of agglomerated and roughly spherical NPS was shown by FESEM images. As seen in the HRTEM images, the nanostructure appears to be aggregated CuO NPs, and the average size of the particle was found to be 18 nm that matched with the XRD analysis. The EDX analysis showed presence of Cu (96.19%) and O (3.81%) in the spectrum. The CuO NPs exhibit significant antibacterial activity against Gram +Ve Staphylococcus *aureus* and Gram −Ve Escherichia *coli* bacteria. Finally, the synthesized CuO nanostructures demonstrate the photocatalytic degradation of Direct Red (DR) and Crystal Violet (CV) dyes under sunlight. The efficiency of degradation within 150 min was determined to be 65% and 88.3%, respectively for DR and CV. This effective removal method under sunlight may support a cost-effective method for degradation of DR and CV dyes from wastewater.

Keywords: Green synthesis, Clitoria ternatea, CuO NPs, Antibacterial-activity, Photocatalytic dye degradation.

1. Introduction

In recent times, the green synthesis of metal oxide (MO) semiconductor nanomaterials has attracted considerable attention because of their extended physical, chemical, and biological properties [1–3]. These significant characteristic properties of MO nanomaterials are employed in various applications in the area of electronics, agriculture, environmental, textile and food packaging industries, etc [4–6].

*Corresponding author:
E-mail address: *prabhucsa@gmail.com* (**S. Prabhu**)

Among the various MOs, CuO is a transition metal oxide, narrow bandgap (~2.0 eV) p-type semiconductor, having a monoclinic crystal structure. It has many unique features such as good stability, excellent thermal conducting nature, large surface area, high electrochemical activity, and better bacterial resistivity [7]. The malleable size, high crystallinity and varied surface morphological behaviour of CuO NPs have empowered their use in diverse applications in batteries, sensors, bio-sensors, active catalyst, energy storage, and solar cells [8,9]. In addition, at increased concentrations, CuO NPs have shown good antibacterial activity by affecting the growth rate of bacteria and killing them. [10,11]. Various methods have been used

to synthesize CuO NPs, including co-precipitation [12], hydrothermal [13] , sonochemical [14], sol-gel [15], electrochemical [16] and microwave-assisted [17]. These synthesis techniques, however, have several drawbacks such as:- reagents are expensive, harmful solvents are used, and the process takes time. As an alternative, bio-based green synthesis is a one-step simple, environmentally-friendly, low-toxic, and cost-effective approach [18]. The green synthesis of CuO NPs using various plants such as Aloe vera [19] , Lantana camara [20] , Hibiscus Rosa [21], and Diospyros montana [22] has been previously reported.

In this investigation, the medicinal flower, *Clitoria ternatea*, was chosen for the synthesis of CuO NPs. *Clitoria ternatea* that belongs to the family of Fabaceae, is commonly known as "Butterfly pea" or "Blue-pea", and originates from South-East Asia and has been distributed throughout the Indian sub-continent [23]. In traditional Ayurvedic medicine, all parts of the plant are commonly used. Its flowers have valuable medicinal properties and are used to treat several diseases such as urinary disorders, wound healing, skin diseases, insect bites, inflammation, fever, body aches and diabetics [24]. *Clitoria ternatea* plant parts have strong antibacterial properties and contain various phytochemicals, including alkaloids, flavonoids, glycosides, phenols, and anthocyanin [25]. These phytochemical compounds serve as strong reducing and capping agents during the synthesis of CuO NPs. The aqueous flower extract is capable of reducing copper sulphate to CuO NPs, and so the NPs thus formed have significant antimicrobial properties. Hence, we examined the possibility of preparing green synthesized CuO NPs using *Clitoria ternatea*, which are suitable for antibacterial applications.

Polluted water is a major environmental hazard. Also, major threatening water pollutants such as dyes, pesticides, and pharmaceuticals are among leading water contaminants [26]. Textile dyes have been increasingly detected in surface water, ground water, and sewage water. MO semiconductors have recently received a lot of attention as a way to oxidise hazardous organic dyes [27,28]. The metal oxide semiconductor interacted photocatalysis is the most efficient degradation processes used for destroying various organic and inorganic toxic pollutants in water [29,30]. Semiconductor-mediated photocatalysis is one of the significant degradation methods among advanced oxidation processes (AOP) for the destroying of toxic organic pollutants are majorly due to the wide bandgap energies and prominent electronic configuration with filled Valence band (VB) and unfilled Conduction Band (CB) [30]. Among the MO semiconductor based

photocatalysts, CuO has been a widely used catalyst because of its high stability, wide band gap, excellent light absorption, quick charge transmission properties, and cost-effective photocatalytic removal of organic toxic pollutants [31,32].

Previous reports demonstrate that the photocatalytic mechanism is a distinctly structure-dependent sensitive major approach in which the oxygen surface lattice of CuO also participates in the mechanism [7]. Earlier studies demonstrated that by using Psidium guajava leaf extract, the green synthesized CuO NPs have the ability to degrade Nile blue and Reactive yellow from aqueous solution [33]. In addition, CuO NPs synthesized using Banana peel extract were tested for their ability to degrade Congo Red dye [34]. However, photocatalytic degradation of hazardous textile dyes of DR and CV using CuO catalyst synthesized from *Clitoria ternatea* flower extracts have not been reported to date. Therefore, in this study the degradation of DR and CV dyes is carried out. Both the DR and CV dyes mostly used in textiles are soluble in water and are found to be toxic. Hence, it is essential to remove such dyes from polluted wastewater. The highlight of our study suggests the use of synthesized CuO NPs could be used as a strong catalytic and significant antibacterial material.

2.Experimental

2.1 Materials

Clitoria Ternatea flowers were picked fresh from the Western Ghats hills, Coimbatore. Copper (II) sulfate pentahydrate ($CuSO_4.5H_2O$) (AR grade) was purchased from Merck. Double distilled water (DW) was used as the solvent for the entire green synthesis procedure.

2.2 Characterization Methods

The XRD pattern of CuO NPs was recorded using Rigaku X-ray Diffractometer with Cu Kα radiation source (λ=0.1542nm) operated at 40 kV. UV–vis absorption spectrum was obtained using Perkin Elmer Lambda 25 spectrometer (JASCO V650). Shimadzu IR Affinity 1S series spectrophotometer was used to obtain the FTIR spectra of the flower extract and CuO NPs. Dynamic Light Scattering (DLS) measurements in a Zetasizer Nano series (Malvern) instrument were used to determine the size distribution and zeta potential values. CuO NPs structural morphology was investigated using Field Emission Scanning Electron Microscope (FESEM) JEOL JEM 6390, Japan while Transmission Electron Microscopy (TEM) with EDX analysis were performed using JEOL 2100, Japan with an acceleration voltage of 200 kV.

2.3 Preparation of Clitoria ternatea flower extract

The *Clitoria ternatea* flower extract was made using the same method as in previous studies [35]. The *Clitoria ternatea* flowers were completely washed three times with DW to remove the dust particles on them, dried at room temperature and cut into small pieces. Afterwards, 10 g of flowers was added with 100 mL of DW and heated at 90 °C for 60 min. The flower extract was allowed to cool to ambient temperature and further filtered by No.1 Whatman filter paper. The collected flower extract solution was kept at 4 °C for further use.

2.4 Synthesis of CuO NPs

The green synthesis of CuO NPs was carried out with slight changes to the procedures described in previous papers. [35]. A 40 mL of 0.1 M CuSO4.5H$_2$O solution was added to 10 mL of 10% *Clitoria ternatea* flower extract. The solution's colour changed from violet to blue, suggesting that CuO NPs had formed. The resulting precipitate was centrifuged for 10 minutes at 5000 rpm, further washed with DW to remove impurities and dried at 80 °C for 4 h. The dried powder was then calcined for 2 hours at 400° C in a muffle furnace. The resultant sample was used for further analysis.

2.5 Antibacterial study

We tested the antibacterial activity of green synthesized CuO NPs using the well diffusion method against Gram + Ve S. aureus and Gram – Ve E. coli bacteria [35]. After spreading the strains on Muller Hinton agar, the samples were allowed to dry for 15 minutes before being placed. The synthesized CuO NPs were taken at three different concentrations (50,100 and 200 μg/μL) and inoculated in the 6 mm diameter well which was prepared by a well borer. After incubating the petri plates at 36 ^{0}C for 24 hours, they were used for bacterial cultural studies. The inhibitory zone was measured and expressed in millimeters.

2.6. Dye degradation Study

As described in previous reports, the photocatalytic degradation activity of CuO NPs was tested under sunlight, with some modifications [36]. DR and CV were used as sample pollutants to investigate the photocatalytic activity of CuO NPs under sunlight. 25 mg of the CuO NPs were added to 25 mL of aqueous dye solution (20 mg/L). The dye solution containing the catalyst was adjusted for pH between 6-8 for maximum adsorption and then the prepared solution was exposed to sunlight for 150 minutes. About 2 mL of the dye solution was taken out at regular intervals of 30 minutes and centrifuged for 10 minutes at 4000 rpm. Further, the degradation efficiency of the reacted solution was analysed using UV–vis absorption spectroscopy. The maximum absorption (λ_{max}) for the DR and CV solutions was measured at 505 and 586 nm, and the C/C_o ratio was determined based on the degradation of the dyes. Photocatalytic experiments were conducted in a cloudless sky between 11:30 a.m. and 2:00 p.m. The measured average solar light intensity was about 0.95 x 10^5 lx.

3. Results and Discussion

3.1 Green synthesis and characterization of CuO NPs

By reducing CuSO$_4$.5H$_2$O with Clitoria ternatea flower extract, CuO NPs are formed. Inset of **Fig. 1** shows the appearance of bluish-green colour and changes in colour due to the formation of different complexes as a result of reduction and oxidation reactions. Active biomolecules present in Clitoria ternatea flower extracts, such as flavonoids, phenols, and anthocyanin, cap copper ions and reduce them to CuO NPs [25].

3.2 UV-Visible spectroscopy

The UV–visible spectra of CuO NPs and flower extract of Clitoria ternatea are shown in **Fig. 1.** The reduction of CuSO$_4$.5H$_2$O into CuO NPs with the addition of aqueous flower extract was identified by the strong distinctive peak at 251 nm. Clitoria ternatea flower extract shows two absorption peaks at 575 and 620 nm, confirming that the extract contains anthocyanin and it is well in agreement with previous reports [37,38].
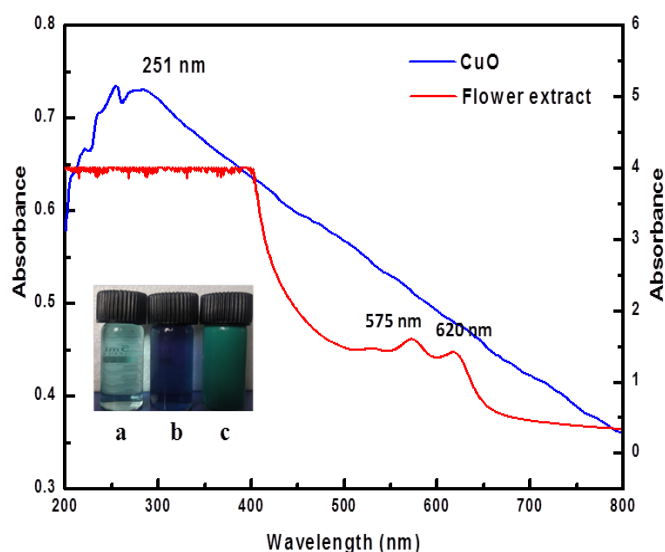
Fig. 1 UV-visible spectrum of *Clitoria ternatea* flower extract and CuO NPs; (in set). (a) Copper sulphate solution, (b) *Clitoria ternatea* flower extract, and (c) CuO NPs.
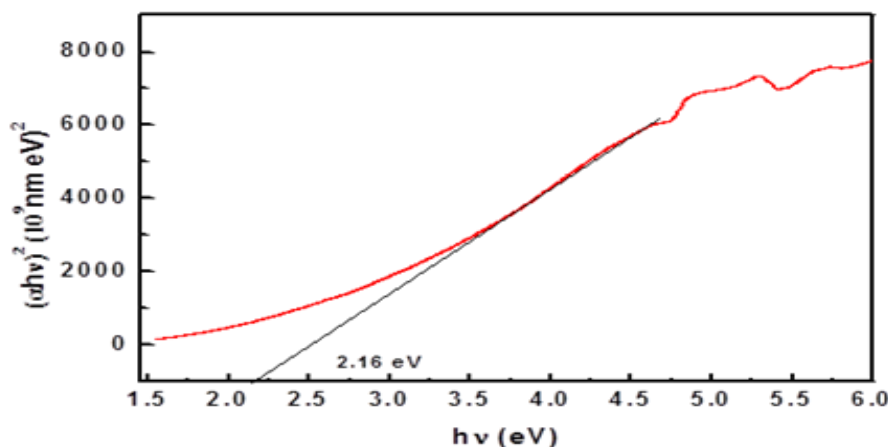
Fig. 2 Optical bandgap of CuO NPs.

The bandgap energy of CuO NPs was calculated using Tauc's Relation, which is given by the following Kubelka-monk [39,40] equation (1),

$$(\alpha h\nu)^n = A (h\nu - E_g) \qquad (1)$$

where, α represents the absorption co-efficient, $h\nu$ is the energy of the incident photon , A is a constant, E_g is the optical band gap energy and n depends on different transitions [39]. The transition values are 1/2 and 2 for allowed direct and indirect electronic transitions, respectively while the values are 3/2 and 3 for forbidden direct and indirect transitions, respectively [41] . The bandgap energy was obtained from the plot between $(\alpha h\nu)^2$ vs. $h\nu$, and was found to be 2.16 eV (**Fig. 2**) which matched with the previous reported values for CuO [41]. It is evident that the obtained absorption edge and band gap shows red shift for multiphase semiconductor catalyst, which confirms that CuO can be used as a catalyst under both visible and UV light irradiation [39].

3.3 FTIR analysis

The FTIR spectrum of the *Clitoria ternatea* flower extract gives information about the various active functional groups responsible for the reduction of copper ions. FTIR spectrum of CuO NPs shows characteristic peaks at 3572, 3487, 1103, 1072, 879, 547 and 490 cm^{-1} (**Fig. 3**). The broad peaks observed at 3572 and 3487 cm^{-1} are assigned to the O-H hydroxyl functional groups [42,43]. The peaks at 1103 and 1072 cm^{-1} correspond to the C-O and C-O-H while peak around 879 cm^{-1} is attributed to the C-H bond [44]. The peaks arising due to the vibrational frequencies of the metal-oxygen (M–O) bond are observed between 400-600 cm^{-1}. The absorption peaks around 547 and 490 cm^{-1} can be assigned to the formation of Cu-O [45]. Likewise, FTIR spectra of the *Clitoria ternatea* flower extract shows peaks that correspond to the various functional groups namely O-H, C-H, C=C, C=O and C-O existing in the flower extract, which is mainly accountable for the reduction of $CuSO_4.5H_2O$ precursor and capping of the CuO NPs [46]. Thus, FTIR spectra confirms that the phytochemicals present in the *Clitoria ternatea* flower extract reduced the precursor and capped the nanoparticles.

3.4 XRD studies

The XRD spectrum of the synthesized CuO NPs is shown in **Fig. 4**. The sharp peaks noticed at 2θ values of $32.5^0, 35.5^0, 38.7^0, 48.9^0, 53.5^0, 61.6^0, 68^0,$ and 72.5^0 are associated with the (110), (002), (111), (202), (020), (113), (220), and (311) planes, respectively and represent the monoclinic crystal structure of CuO (JCPDS standard no. 76-1467), that is matched with the previous findings [47]. The highly crystalline and sharp diffraction peaks demonstrate that CuO is pure and well arranged in specific orientation [48-49]. The crystallite size of the CuO NPs was calculated using the Scherer frmula from equation (2);

$$d = \frac{K\lambda}{\beta \cos \theta} \qquad (2)$$

where, d represents the average crystallite size, K is the Scherer constant (0.9), λ indicates the wavelength of X-ray radiation, and β represents the full-width half maximum (FWHM) [50] . The average crystallite size of the CuO NPs was calculated to be 17 nm. The size of CuO NPs calculated matches that in the previous findings [51].
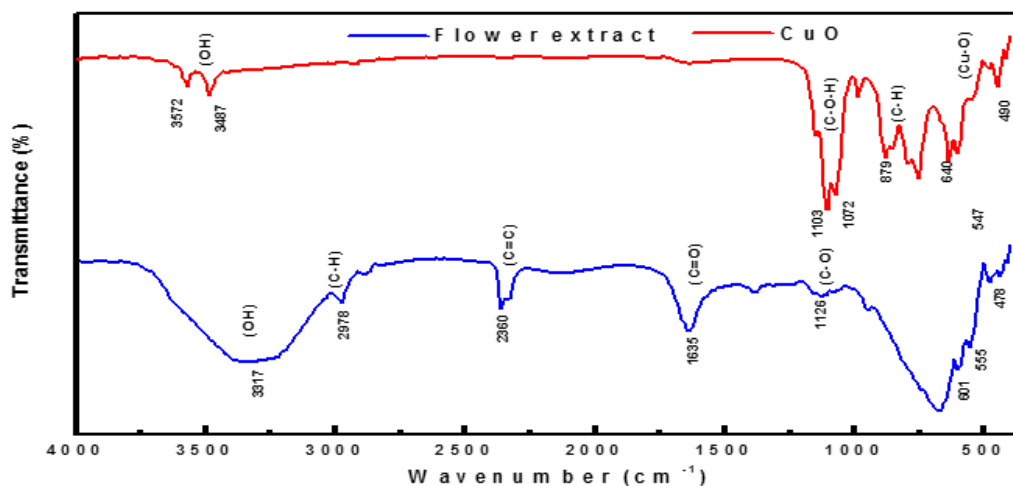
Fig. 3 FTIR analysis of *Clitoria ternatea* flower extract and CuO NPs.
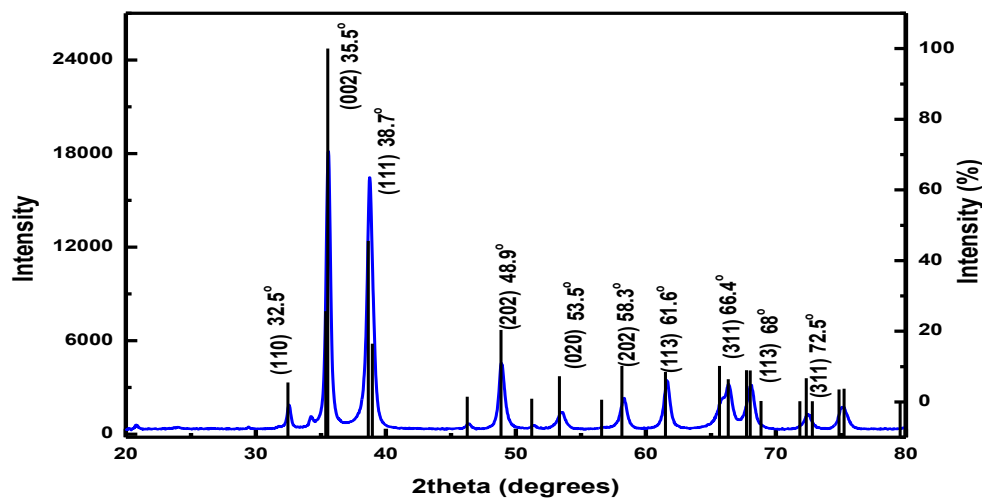

Fig. 4 XRD Pattern of CuO NPs

3.5 Dynamic Light Scattering analysis (DLS)

The size, surface charge, and stability of the NPs was determined by DLS measurements. The synthesized CuO NPs had an average particle size of 88 nm and zeta deviation was -17.4 mV as shown in **Fig. 5a** and **5b**. These larger CuO NPs are a result of the surrounding of the water layer on the surface of the NPs. Furthermore, it demonstrates the moderate stability and capping of the flower extract *Clitoria ternatea* wherein biomolecules are adsorbed on to the surface of CuO NPs. The result revealed that the higher particle size (88nm) and negative value of zeta potential (-17.7 mV) denoted the strong repulsion force between the particles indicating quality and stability in water medium. Particles were agglomerated due to the weak van der Waals interaction

[51]. The particle size and charge distribution of CuO NPs appear to improve their biological-based properties [52].

3.6 FESEM studies

The size and morphological characterization of the synthesized CuO NPs were performed using FESEM. The FESEM images reveal that the CuO NPs have spherical morphology and there is agglomeration between particles (**Fig. 6**). The average particle size was found in the range of 60-80 nm. The agglomeration depends on sample preparation, hydrophobic magnetism and electrostatic field interaction and is further corroborated by DLS studies (88 nm) [53]. The results are in close agreement with those of previously synthesized CuO NPs. [54].
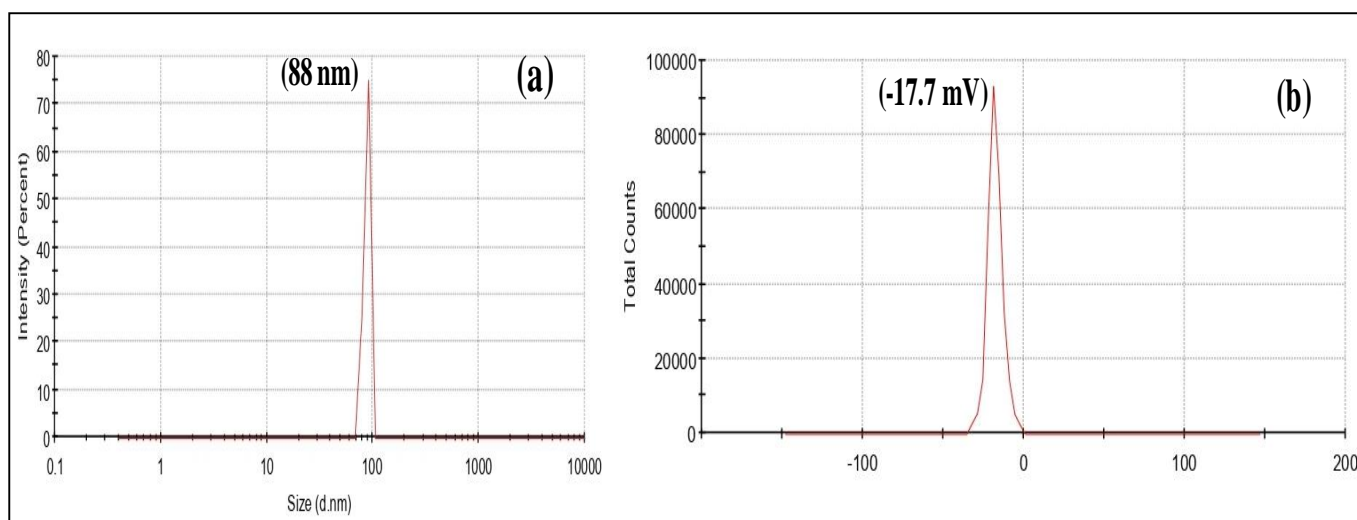
**Fig. 5** (a) DLS, (b) zeta potential analysis of green synthesized CuO NPs.
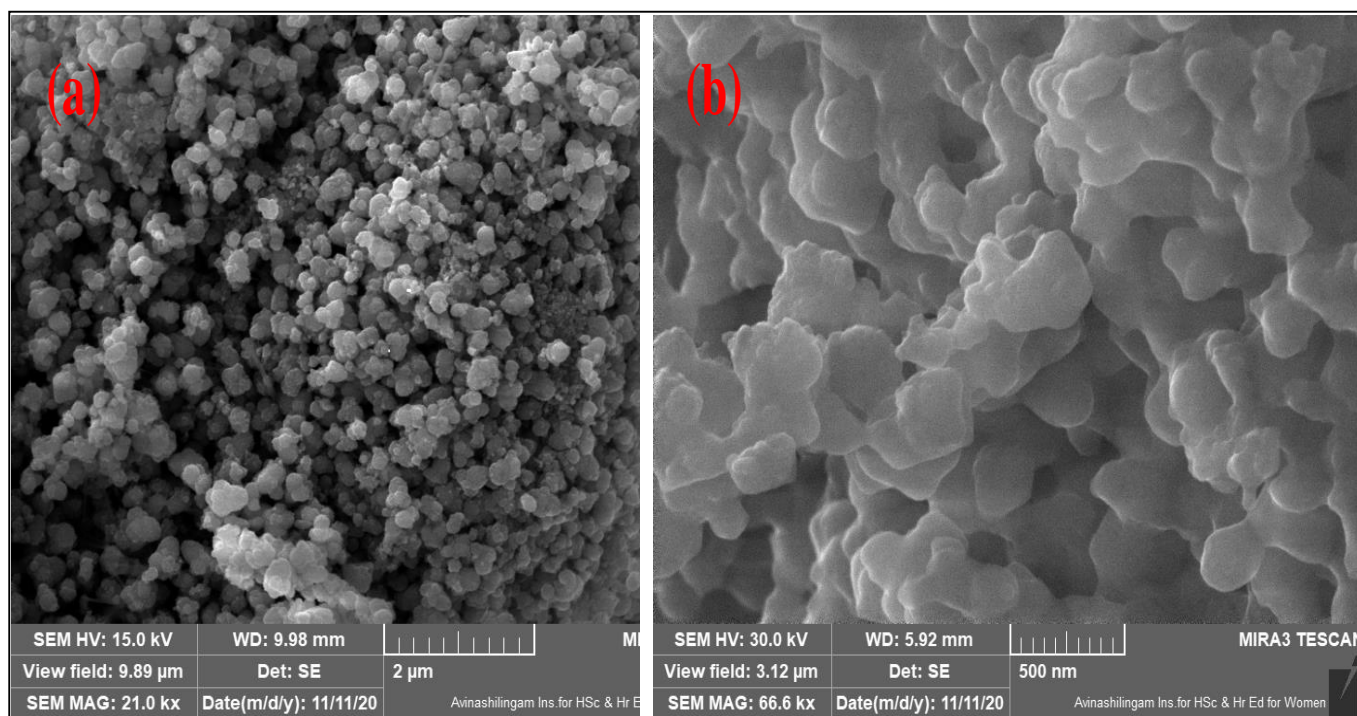
**Fig. 6** FESEM micrographs of CuO NPs

3.7 HRTEM studies

In order to demonstrate the size and morphology of the synthesized CuO NPs, HRTEM micrographs have been recorded at two magnifications, 200 and 50 nm, as shown in **Fig. 7a** and **7b**. Accordingly, the surface of the particles was roughly spherical in shape, with aggregated and stacked NPs in groups. The TEM histogram showed the average particle size of 18 nm (**Fig. 7c**) and these results are very similar to the average crystallite size determined by Scherrer's formula (17.46 nm). The selected area electron diffraction (SAED) in **Fig. 7d** shows the diffraction rings that are concentric circles. This proves the crystalline nature of CuO NPs and matched with XRD results [51]. The EDS analysis shown in **Fig. 8** confirmed the presence of Cu and O elements. CuO NPs had 96.19% of Cu and 3.81% of O. Further, the atomic percent of Cu was found to be 86.42 and O as 13.58 and there is no evidence for the presence of additional impurities. According to the EDX result, the presence of copper (Cu) element was found to be higher and is attributed to the use of copper grid for the EDX analysis. The smaller sized particles (18 nm) have a larger surface area with more reactive centres that support the reaction and could improve the photocatalytic properties of the NPs [55].
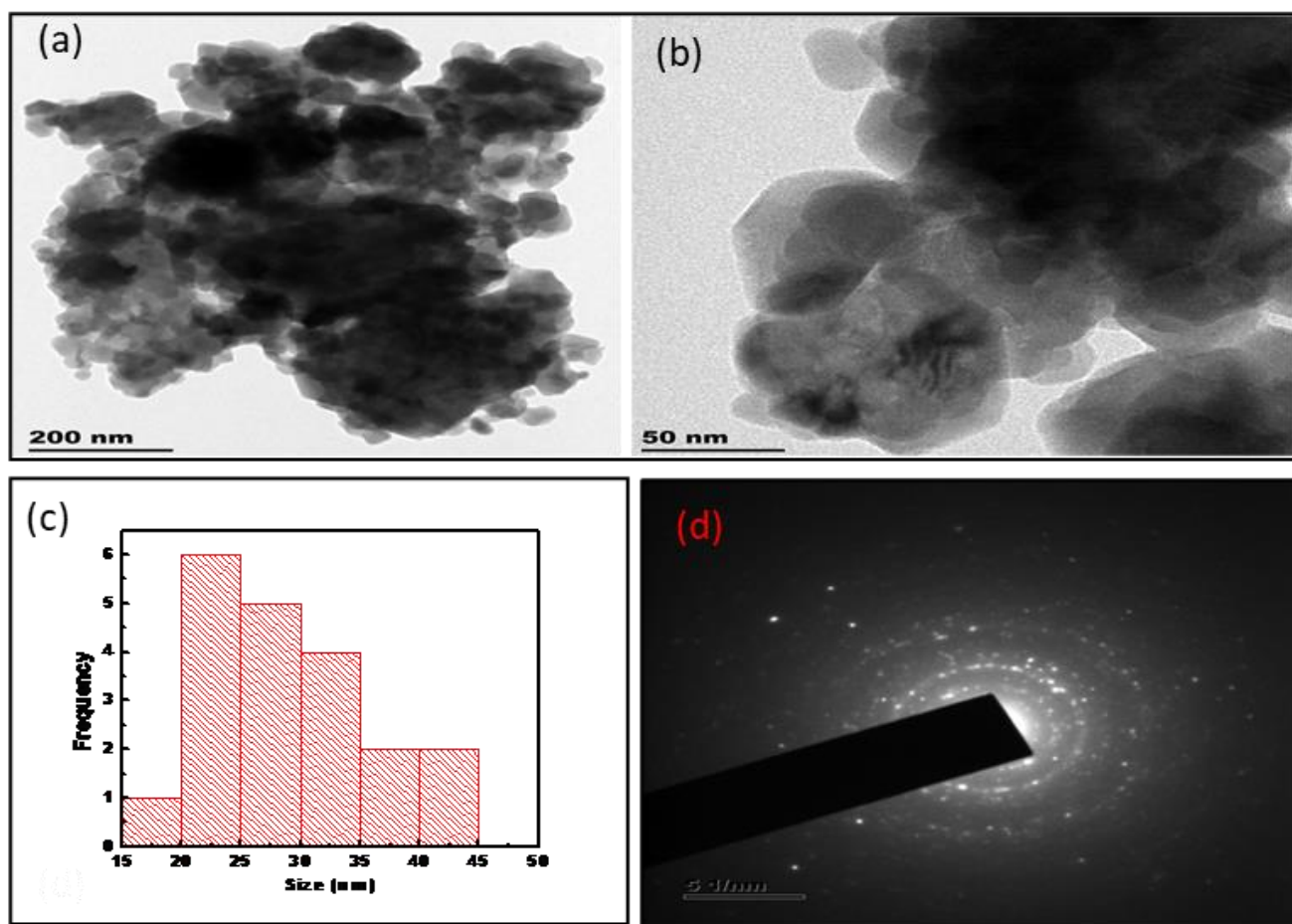
**Fig. 7** HRTEM micrograph of CuO NPs (a) 200 nm, (b) 50 nm (c) size distribution histogram, (d) SAED pattern
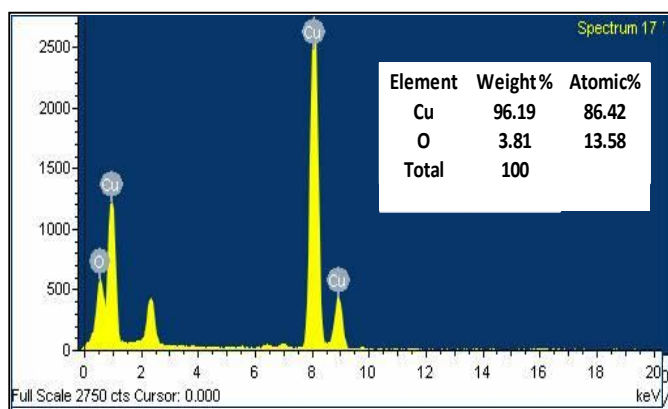
Fig. 8 EDS spectrum of CuO NPs

3.8 Antibacterial studies

The antibacterial activities of the CuO NPs were analysed against S. aureus and E.coli bacteria using the well diffusion method shown in **Fig. 9a** and **9b** [33]. Based on the results, the zone of inhibition increased with increasing concentrations of CuO NPs (50, 100, and 200 μg/mL) and is shown in **Fig. 9c**. For *E. coli*, the highest zone of inhibition was measured as 23±1.0 mm and *S. aureus* measured as 20±1.0 mm for 200

μg/mL. Similarly, the minimum zone of inhibition for *S. aureus* was found to be 16± 1.0 mm and that for *E. coli* was 15± 1.0 mm at 50 μg/mL (**Table 1**). CuO NPs produce reactive oxygen species (ROS), which trigger the cellular oxidative metabolism and kill bacteria by breaking down the cell wall and destroying their DNA [43]. The CuO NPs showed significant antibacterial activity against both S. aureus and *E. coli* bacteria, but higher efficiency was noticed against *E. coli* bacteria. Antibacterial activity depends on the cell wall and membrane characteristics of gram + ve and gram -ve bacteria. The gram + ve bacteria have a broader cell wall and membrane than gram – ve bacteria. According to earlier reports on CuO NPs, it has been proved that Copper ions would cause DNA breakdown and reduce bacterial activities. The CuO-NPs would destroy bacterial cell walls and cause membrane breakage, thus killing the bacteria [43]. It was remarkable to note that the concentrations of CuO NPs increase as well as the zone of inhibition. The factors such as powder concentration, particle size, and large surface area influence the antibacterial activity of CuO NPs. Thus, the present study suggests that NPs with high crystalline nature and smaller particle size (17 nm) could possess high antibacterial activity [56].
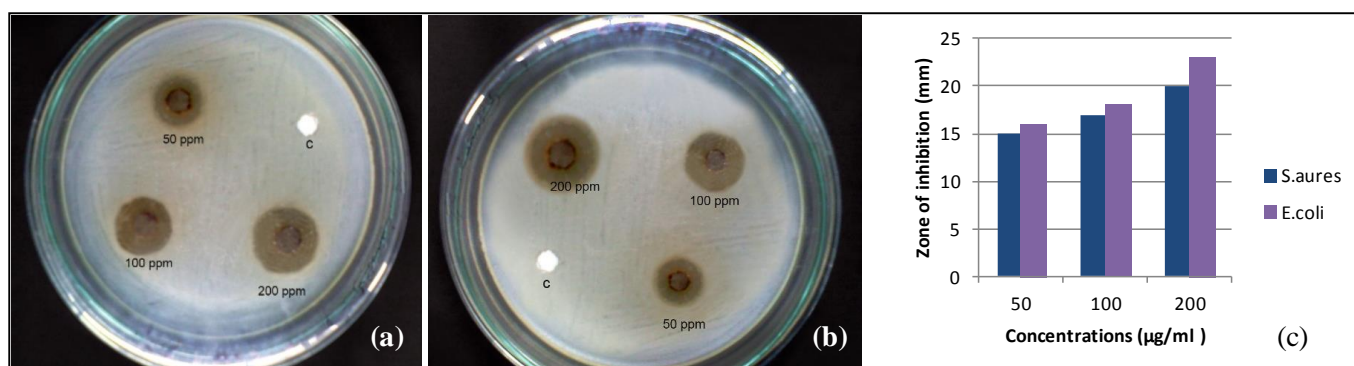
Fig. 9 Antibacterial activity of CuO NPs at different concentrations against (a) *S. aureus* and (b) *E. coli,* (c) Bacterial zone of inhibition

Table 1 Antibacterial activity of CuO NPs on *E. coli* and *S. aureus*

Bacteria	Zone of inhibition in (mm)		
	50μg/mL	100 μg/mL	200 μg/mL
E. coli	16 ± 1.0	18 ± 1.0	23± 1.0
S. aureus	15± 1.0	17. ± 1.0	20± 1.0

3.9 Dye degradation Studies

As another main objective of this study, some environmental toxic organic pollutants such as CV and DR dye solutions were selected to investigate the degradation efficiency of CuO NPs under sunlight. **Fig. 10a** and **10b** show the UV-vis absorption spectra for the degradation of DR and CV dyes at appropriate time intervals under sunlight. When sunlight irradiates the DR and CV dye solutions containing the catalyst, the dyes are visibly reduced. The photocatalytic degradation was analysed by UV-visible spectrum. The maximum absorbance (λmax) of the DR and CV dyes were found to be 507 and 586 nm, respectively which decreases gradually, indicating a strong reduction of the DR and CV dyes. The red and violet colour of the dyes disappear confirming that the chemical arrangement of dye molecules has collapsed and ruptured. The degradation efficiencies of the DR and CV dyes are calculated using the Beer Lamberts equation (3)

$$D(\%) = \frac{C_0 - C}{C} \times 100 \qquad (3)$$

where, D is the efficiency of degradation, C_0 and C represent the initial and final absorbance of dye solution. The total dye degradation percentages of DR and CV dyes were found to be 65% and 88.3%, respectively.

Fig. 11 shows the mechanism of photocatalytic degradation process of DR and CV dye solutions under sunlight irradiation. In the process of dye degradation under sunlight, free electrons shift from the valence band (VB) to the conduction band (CB) with the exposure CuO semiconductor is further led too electron-hole pair formation which in turn produce superoxide radical anion (O_2^-) and hydroxyl radicals ($^\bullet$OH) in the presence of H_2O and O_2 molecules. The efficiency of photodegradation has a major role on the formation of hydroxyl radicals, which are essential species in the process of degradation [54]. The dye degradation mechanism is as follows:

$$CuO + h\upsilon \rightarrow h^+ + e^- \qquad (4)$$

$$h^+ + OH^- \rightarrow OH \qquad (5)$$

$$e^- + O_2 \rightarrow O_2^- \qquad (6)$$

$$OH^- / O_2 + dyes \rightarrow \text{Degraded products} \qquad (7)$$

Fig. 10c show the kinetic degradation for DR and CV dyes and the graph shows correlation coefficients (R^2) values of 0.983 and 0.906, which confirms that the photocatalytic degradation of DR and CV dyes fits with the pseudo-first order reaction kinetics. Photodegradation reaction satisfied the Hinselwood equation [40,57]

$$\ln\left(\frac{C}{C_0}\right) = -kt \qquad (8)$$

where k denotes the photo degradation rate constant (min^{-1}) and t represents the reaction time (min). The value of -ln (C/C_0) vs time (t), represents linear relationship. In **Fig. 10d**, the kinetic constants (k) calculated from the photodegradation of CuO catalyst were 0.0150 and 0.0301 min^{-1}, respectively. The kinetic
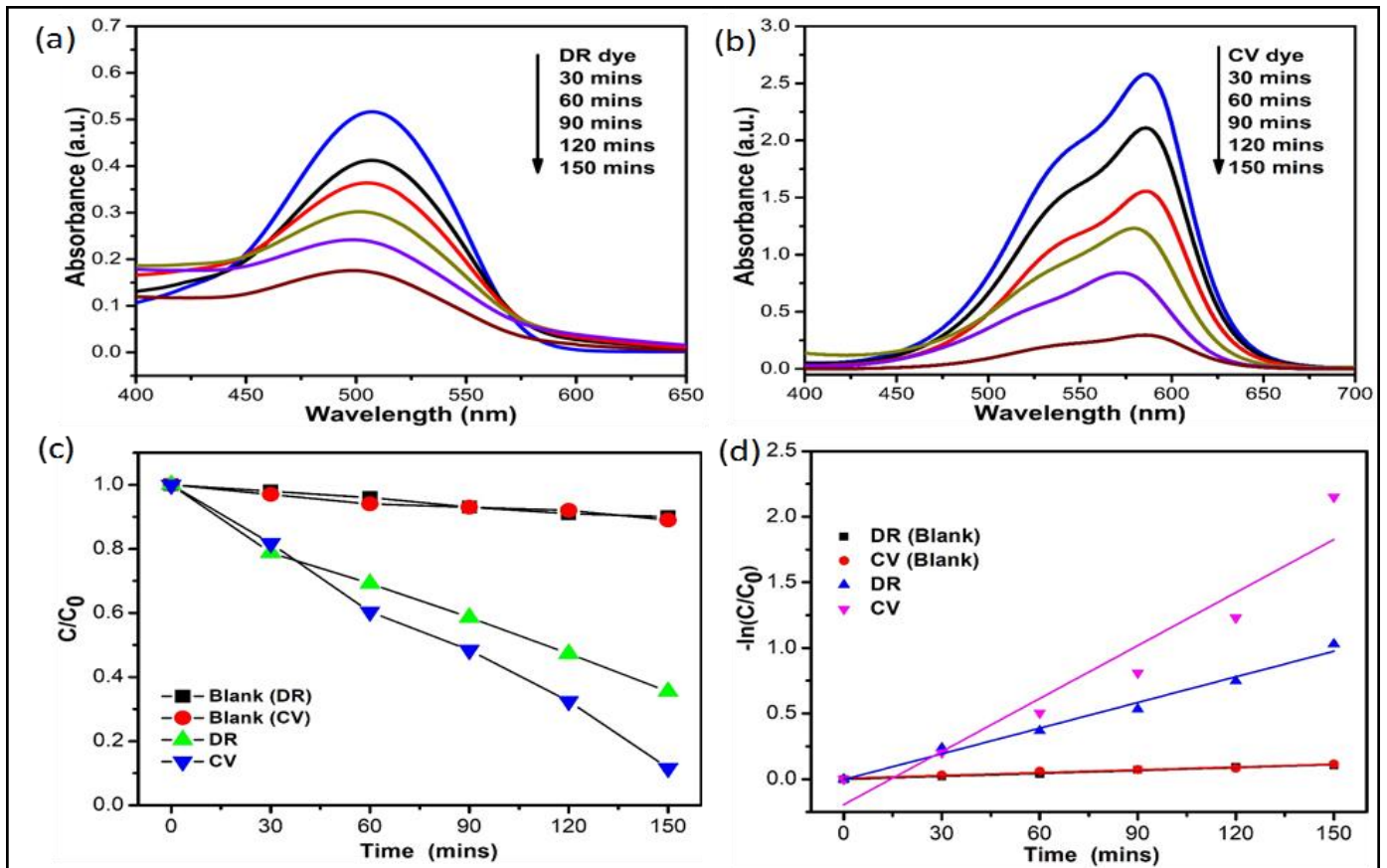
Fig. 10 (a&b) Photo degradation of DR and CV dye by CuO NPs, (c&d) Kinetic degradation data under sunlight.
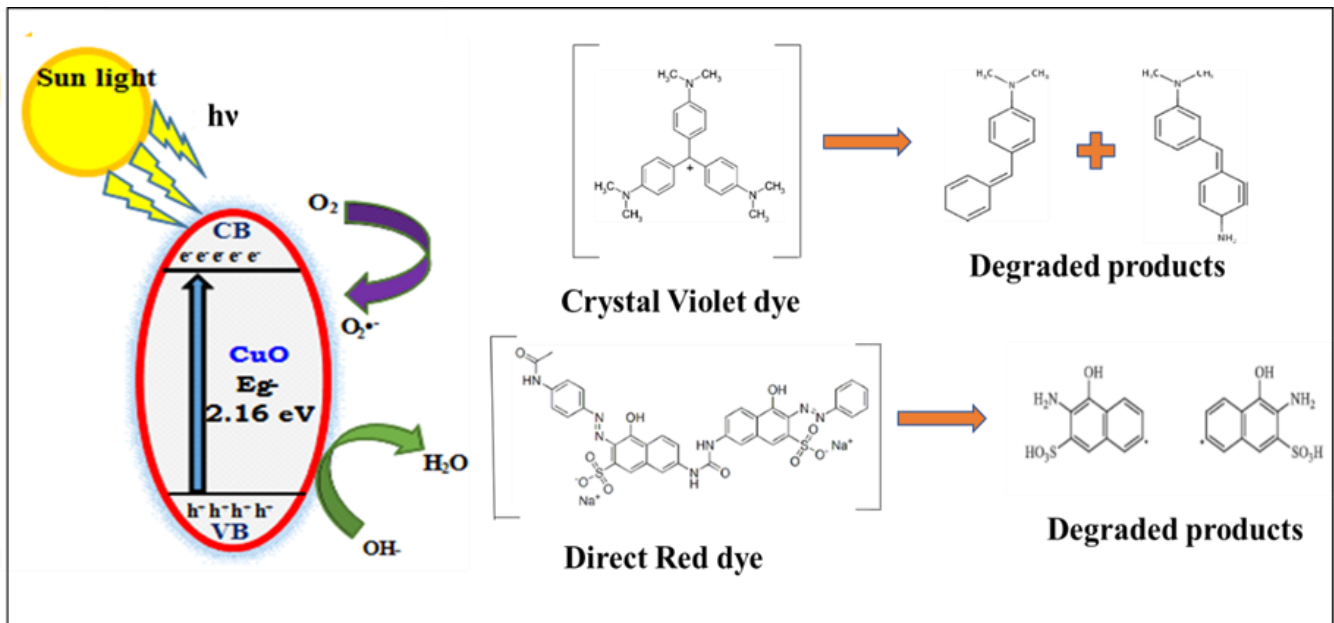

Fig. 11 Mechanism of photocatalytic degradation against CV and DR dyes by CuO NPs under sunlight.

constants (k) showed that the CuO catalysts had better performance for CV dye when compared with DR dye photodegradation under the sun light. **Table. 2** contains the values of dye degradation efficiency, k and R^2. In this case, the degradation efficiency of the DR and CV values can be attributed to the small size of the particle and large surface area-to-volume ratio compared to their bulk counterparts, enabling higher photon absorption on the photocatalyst surface [31].The dye concentration, catalyst, incident light intensity, and irradiation time influence the dye degradation approach [58].

Table 2 Photocatalytic activity studies of CuO NPs

S. No	Dye	Band gap value (eV)	Dye degradation efficiency (%) (150 min)	Photo degradation rate constant k (min^{-1})	Corelation co-efficient (R^2)
1	Direct Red	2.16	65.0	0.0150	0. 983
2	Crystal Violet	2.16	88.3	0.0301	0.906

4. Conclusions

This study provides a distinctive approach for the green synthesis of CuO NPs by using flower extract of *Clitoria ternatea* for the first time. The Green synthesis method that takes advantage of using flower extract from a medicinal plant is cost effective and eliminates the need for toxic chemical reducing agents. XRD and FTIR results corroborates the formation of CuO NPs, which exhibited the pure crystalline of CuO that showed enhanced performance in antibacterial studies and photocatalytic activity. CuO NPs demonstrate significant inhibition activity against *E. coli* and *S. aureus* bacterial strains, but superior efficiency was noticed against gram-ve *E. coli*. The synthesized CuO NPs can be used as significant photocatalyst in the degradation of dyes DR and CV under sunlight. These are found to follow pseudo first order kinetics. It is concluded that the results elucidate the potential of CuO NPs synthesized from Clitoria ternatea flower extract as a significant antibacterial and catalytic agent. The results prove that the synthesized CuO NPs using *Clitoria ternatea* flower extract were found to be significant antimicrobial and catalytic agents. By large-scale green synthesis, CuO NPs could be used to treat wastewater, environmental remediation, and selectively kill bacteria.

References

[1] N.H.A. Nguyen, V.V.T. Padil, V.I. Slaveykova, M. Cernik, A. Sevcu, , Nanoscale Res. Lett. 13 (2018) 1-13.

[2] M.S. Chavali, M.P. Nikolova, SN Appl. Sci. 1 (2019) 1-30.

[3] H. Derikvandi, A. Nezamzadeh-Ejhieh, J. Hazard.Mater.321 (2017) 629-638.

[4] G. Ali, Y.J. Park, J.W. Kim, S.O. Cho, ACS Appl. Nano Mater. 1 (2018) 6112–6122.

[5] M. Giahi, A. Hoseinpour Dargahi, Iran. J. Catal.6 (2016) 381-387.

[6] Hamid Reza Pouretedal, Mohammad Fallahgar, Fahimeh Sotoudeh Pourhasan, Mohammad Nasiri, Iran. J. Catal. 7 (2017) 317-326.

[7] S.Saranya S, R.Agneeswaran , P.N.Deepa, ACS Omega. 5 (2020) 1040–1051.

[8] Haffsa Siddiqui, M.S. Qureshi, Fozia Zia Haque, Nano-Micro Lett. 12:29 (2020) 1-12.

[9] Zahra Amani, A. Nezamzadeh-Ejhieh, J. Colloid Interf.Sci.504 (2017) 186-196.

[10] D. Manyasree, K.M. Peddi, R. Ravikumar, Int. J. Appl. Pharm. 9 (2017) 71–74.

[11] M.S. Jadhav, S. Kulkarni, P. Raikar, D.A. Barretto, S.K. Vootla, New J. Chem. 42 (2018) 204–213.

[12] A.A. Bhat, B.A. Thoker, A.K. Wani, G.A. Sheergojri, M.A. Kaloo, B.A. Bhat, S.M. Ahmad Rizvi, Chem. Sci. Eng. Res. 3(6) (2021) 25-29.

[13] M. Outokesh, M. Hosseinpour, S.J. Ahmadi, T. Mousavand, S. Sadjadi, W. Soltanian, Ind. Eng. Chem. Res. 50 (2011) 3540–3554.

[14] N. Silva, S. Ramírez, I. Díaz, A. Garcia, N. Hassan, Materials (Basel). 12 (2019) 1–13.

[15] L. Dorner, C. Cancellieri, B. Rheingans, M. Walter, R. Kagi, P. Schmutz, M. V. Kovalenko, L.P.H. Jeurgens, Sci. Rep. 9 (2019) 1–13.

[16] R. Katwal, H. Kaur, G. Sharma, M. Naushad, D. Pathania, J. Ind. Eng. Chem. 31 (2015) 173–184.

[17] P. Sutradhar, M. Saha, D. Maiti, J. Nanostructure Chem. 4 (2014) 4–9.

[18] A. Rastogi, M. Zivcak, O. Sytar, H.M. Kalaji, X. He, S. Mbarki, M. Front. Chem. 5 (2017) 1–16.

[19] S. Sharma, K. Kumar, A, J. Dispers. Sci. Technol. (2020) 1–13.

[20] Rakesh Chowdhury, Aslam. Khan, Md. Harunar Rashid, RSC Adv. 10 (2020) 14374–14385.

[21] Rajendran . A, Siva. E, Dhanraj C, Senthilkumar S, J. Bioprocess. Biotech. 8 (2018) 10003248.

[22] K.S. Siddiqi, M. Rashid, A. Rahman, Tajuddin, A. Husen, S. Rehman, Agric. Food Secur. 9 (2020) 1–15.

[23] G.K. Oguis, E.K. Gilding, M.A. Jackson, D.J. Craik, Front. Plant Sci. 10 (2019) 1–23.

[24] N. Jamil, F. PaEe, AIP Conf. Proc., AIP, Inc. 2002 (2018) 020044-45.

[25] Chakraborthy GS, Kumar V, Gupta S, Kumar A, Gautam N, Kumari L, J. Appl. Pharm. Sci. Res. 1 (2018) 3–9.

[26] Hadis Derikvandi, Alireza Nezamzadeh-Ejhieh, J. Colloid Interface Sci. 490 (2017) 652–664.

[27] Somayeh Dianat, Iran. J. Catal.8(2) (2018) 121-132.

[28] Alireza Nezamzadeh-Ejhieh, Zahra Salimi, Desalination. 280 (2011) 281–287.

[29] Shirin Ghattavi, Alireza Nezamzadeh-Ejhieh, Composites Part B. 183 (2020) 107712.

[30] Akbar Rostami-Vartoonia, Abolfazl Moradi-Saadatmanda, Mojtaba Bagherzadehb, Mohammad Mahdavic, Iran. J. Catal. 9 (2019) 27-35.

[31] S. Dharmraj Khairnar, M. Rajendra Patil, V. Shankar Shrivastava, Iran. J. Catal. 8 (2018) 143-150

[32] A. Sobhani-Nasab, M. Eghbali-Arani, S. Mostafa Hosseinpour-Mashkani, Ahmadi, M Rahimi-Nasrabadi, Vahid Ameri, Iran. J. Catal.10(2), 2020, 91-99

[33] S. Sathiyavimal, S. Vasantharaj, V. Veeramani, M. Saravanan, G. Rajalakshmi, T. Kaliannan, F. J. Environ. Chem. Eng. 9 (2021) 105033.

[34] M. Aminuzzaman, L.M. Kei, W.H. Liang, AIP Conf. Proc. 1828 (2017) 0200161-165.

[35] S. Prabhu, T.D. Thangadurai, P.V. Bharathy, Green-based Biosynthesis of Zinc Oxide Nanoparticles Using Clitoria ternatea Flower Extract and Its Antibacterial Activity, Nano Biomed. Eng. 13 (2021) 394-400.

[36] N. Venkatesh, S. Aravindan, K. Ramki, G. Murugadoss, R. Thangamuthu, P. Sakthivel, Environ. Sci. Pollut. Res. 28 (2021) 16792–16803.

[37] B. Kumar, K. Smita, L. Cumbal, A. Debut, Y. Angulo, J. Saudi Chem. Soc. 21 (2017) S475–S480.

[38] N.A. Ludin, M.A.M. Al-Alwani, A.B. Mohamad, A.A.H. Kadhum, N.H. Hamid, M.A. Ibrahim, Int. J. Electrochem. Sci. 13 (2018) 7451–7465.

[39] Hadis Derikvandi, Alireza Nezamzadeh-Ejhieh, J. Photochem.Photobiol. A: Chem. 348 (2017) 68-78.

[40] Meymanat Mehrali-Afjani, Alireza Nezamzadeh-Ejhieh, Hamidreza Aghaei Chem. Phys. Lett. 759 (2020) 137873.

[41] Manikandan Balakrishnan, Rita John, Iran. J. Catal.10 (2020) 1-16.

[42] W.W. Andualem, F.K. Sabir, E.T. Mohammed, H.H. Belay, B.A. Gonfa, J. Nanotechnol. 2 (2020) 1-10

[43] S. Sathiyavimal, S. Vasantharaj, D. Bharathi, M. Saravanan, E. Manikandan, S.S. Kumar, A. Pugazhendhi, J. Photochem. Photobiol. B Biol. 188 (2018) 126–134.

[44] Salma .A. Al-Tamimi, Green Chem. Lett. Rev. 14 (2021) 165–178.

[45] N. Krithiga, A. Rajalakshmi, A. Jayachitra, J. Nanosci. 2015 (2015) 1–8.

[46] D. Khwannimit, R. Maungchang, P. Rattanakit, Int. J. Environ. Anal. Chem. 10 (2020) 1–17.

[47] Alireza Nezamzadeh-Ejhieh, Shohreh Hushmandrad, Appl. Catal. A Gen. 388 (2010) 149–159.

[48] Ailin Yousefi, Alireza Nezamzadeh-Ejhieh, Mehrosadat Mirmohammadi, Environ. Technol. Innov. 22 (2021) 101496.

[49] G. Kausalya, N. Manjubaashini, P. Jerome, R. Karvembu, T. Daniel Thangadurai, Mater. Lett. 185 (2016) 218–221.

[50] M. Arun Kumar, A. Samson Nesaraj, Iran. J. Catal.10 (2020) 235-245.

[51] P. Yugandhar, T. Vasavi, P. Uma Maheswari Devi, N. Savithramma, Appl. Nanosci. 7 (2017) 417–427.

[52] S.C. Mali, A. Dhaka, C.K. Githala, R. Trivedi, Biotechnol. Reports. 27 (2020) e00518.

[53] A.D. Mahmoud, K.M. Al-Qahtani S.O. Alflaij, S.F. Al-Qahtani, F.A. Alsamhan, Sci. Rep. 11 (2021)1–13.

[54] M. Ali, M. Ijaz, M. Ikram, A. Ul-Hamid, M. Avais, A.A. Anjum, Nanoscale Res. Lett. 16 (2021) 1-13.

[55] Alireza Nezamzadeh-Ejhieh, Zohreh Banan, Desalination. 279 (2011) 146-151.

[56] H.R. Naika, K. Lingaraju, K. Manjunath, D. Kumar, G. Nagaraju, D. Suresh, H. Nagabhushana, J. Taibah Univ. Sci. 9 (2015) 7–12.

[57] Ailin Yousefi, Alireza Nezamzadeh-Ejhieh, Iran. J. Catal.11 (2021) 247-259

[58] N. Sreeju, Alex Rufus, Daisy Philip, J. Mol. Liq. 242 (2017) 690–700.